Through the thick and thin: New constraints on Mars paleopressure history 3.8 – 4 Ga from small exhumed craters

A.O. Warren[1], E.S. Kite[1], J.-P. Williams[2], B. Horgan[3] aowarren@uchicago.edu
[1]University of Chicago, Department of Geophysical Sciences; [2]UCLA Department of Earth, Planetary and Space Sciences; [3]Purdue University, Department of Earth, Atmospheric, and Planetary Sciences

1. Introduction

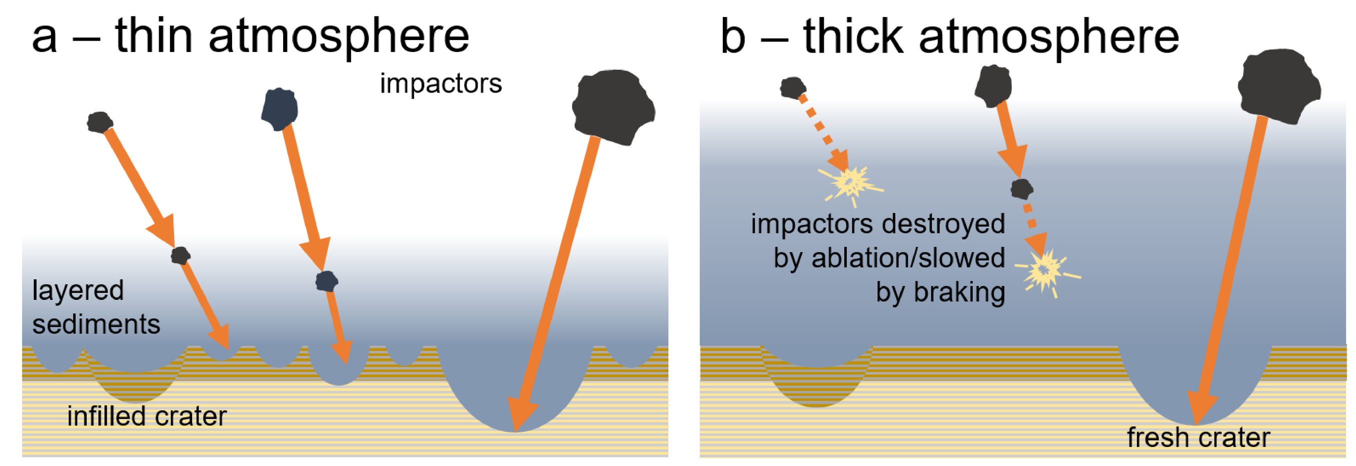

Figure 1. Schematic illustration of cratering due to impactors passing through a a) thin atmosphere, b) thick atmosphere, also showing infill of ancient craters by layered sediments ("infilled crater"). The thin atmosphere case has a much higher proportion of smaller craters than the thick atmosphere case.

Changes in Martian atmospheric pressure over time are an important control on Mars' climate evolution[1]. A direct method for estimating paleopressure uses the size frequency distribution of small, ancient craters to estimate an upper limit on atmospheric pressure[2,3]. **Thin planetary atmospheres allow small objects to reach the surface at high velocities, forming a greater proportion of small impact craters[4] (Fig 1).** Finding paleopressure estimates for sites of multiple ages gives us better temporal coverage of paleopressure evolution. Here we report paleopressure data for 2 new sites in **Mawrth Vallis** and **Meridiani Planum.**

2. Methods

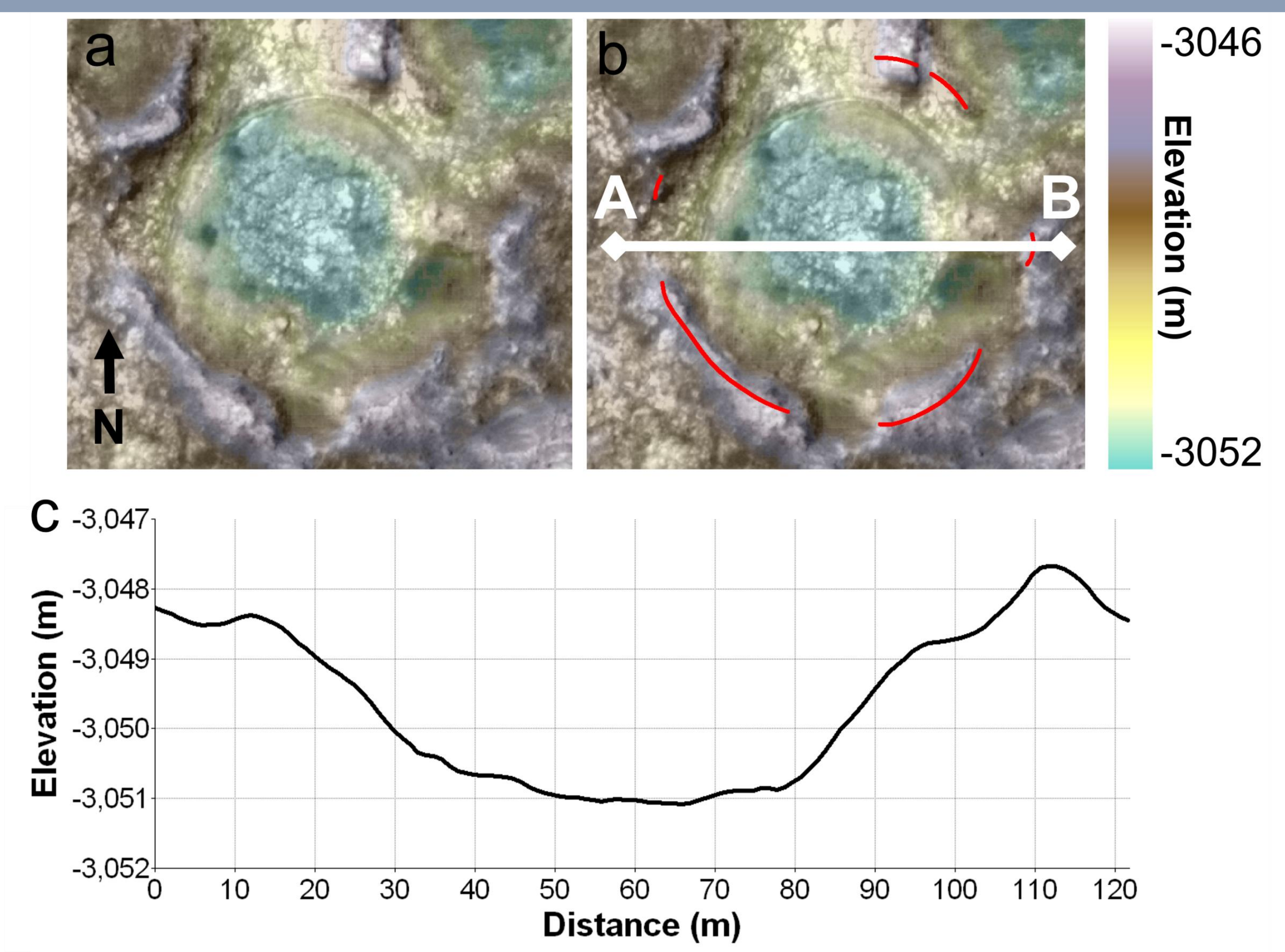

Figure 2. Example ancient embedded crater on Mawrth paleosurface: a) No interpretation, b) topographically elevated rim outlined in red, c) cross section showing depth <<0.2× diameter. Solar incidence angle 45°.

The **Mawrth phyllosilicates** are the oldest known hydrously altered sedimentary rocks in the Solar System (4-3.8 Ga[5]), suggesting surface temperatures >273K[6]. The phyllosilicates overlie an older (>4 Gyr) **paleosurface**[5] with a high density of exhumed craters. Our **Meridiani Planum** site (~3.8 Ga[7]) features sedimentary units indicative of surface liquid water during deposition[8]. We use HiRISE orthoimages, anaglyphs, and digital terrain models (DTMs) to identify exhumed ancient craters at our 2 sites (Fig 2) and compare the size-frequency distribution of measured crater populations to predictions from an atmosphere-impactor inter-action model[9] for atmospheres of different pressures[2] (Fig 3).

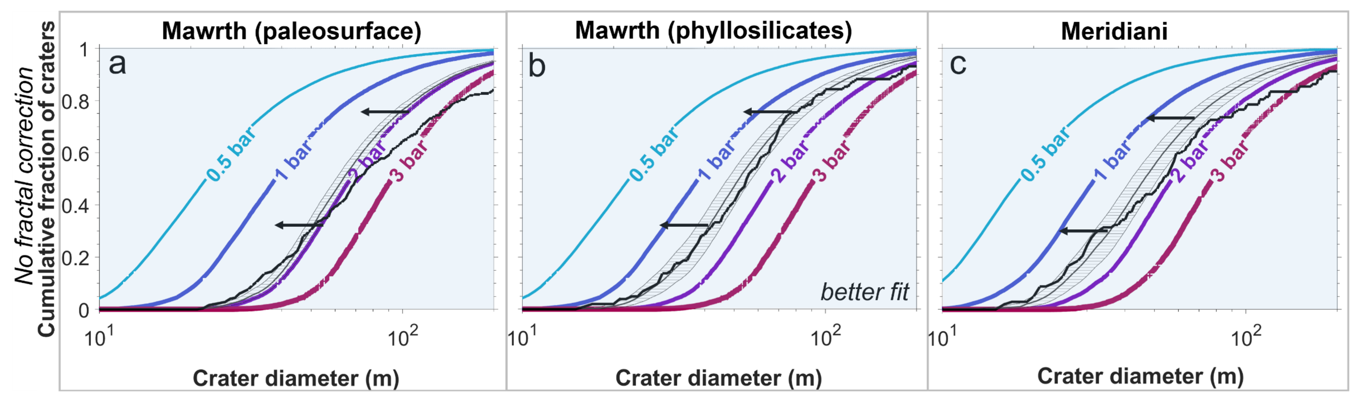

Figure 3. Fits of measured CSFDs (black) to synthetic data from atmosphere-impactor interaction model (colored lines) for the Mawrth paleosurface (a), Mawrth phyllosilicates (b), and Meridiani (c). x-axis upper limit is 200m because fitting procedure is most sensitive to smallest craters in distribution (15-50m. Hatched areas show 2-σ bootstrap error envelope on fit. Black horizontal arrows indicate that paleopressure fits are upper bounds.

Our new upper limits on paleopressure are <(1.9±0.1) bar at/before 4 Ga (Mawrth paleosurface) and <(1.5±0.1) bar at ~3.8 Ga (Mawrth phyllosilicates/Meridiani) (Fig 4).

3. Results

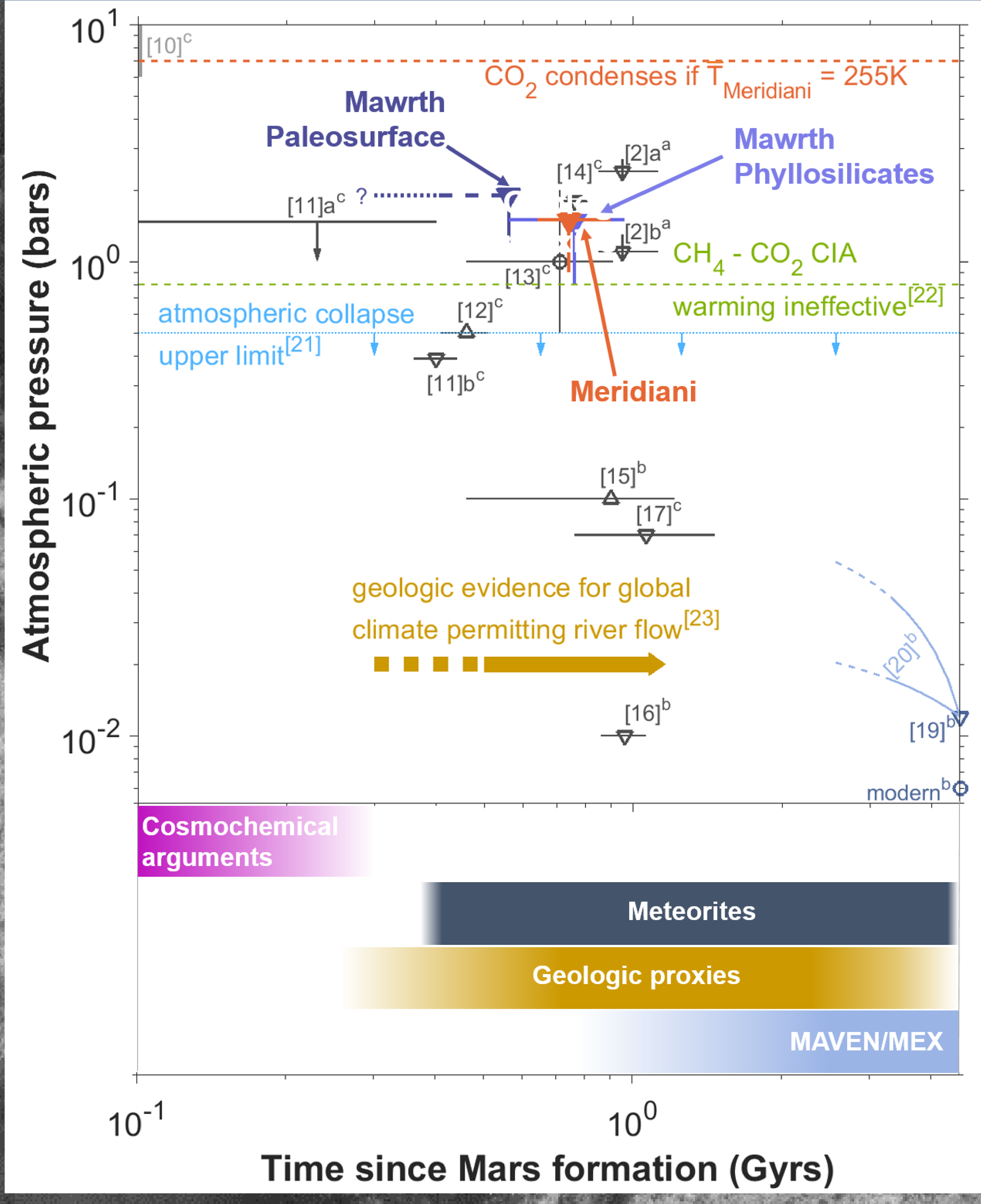

Figure 4. Updated paleopressure constraints for Mars. Numbers correspond to reference list. Superscripts: a – constraints from exhumed ancient craters, b remote sensing, c - all other meth-ods. [17]c (since superseded by experimental results, see [18]), modernb - annual mean modern atmospheric pressure. Modern MAVEN O loss rates [20]b (assumed all due to CO2) extrapolated backwards in time. Colored bars - approximate temporal extent of methods for constraining paleopressure. Upward/downward facing triangles indicate lower/upper bounds. Circles – estimates of absolute atmospheric pres-sure/direct measurements. Bars with an arrow indicate peri-ods of time (rather than points) for which pressure had to be continuously below a certain value.

4. Crater population modification

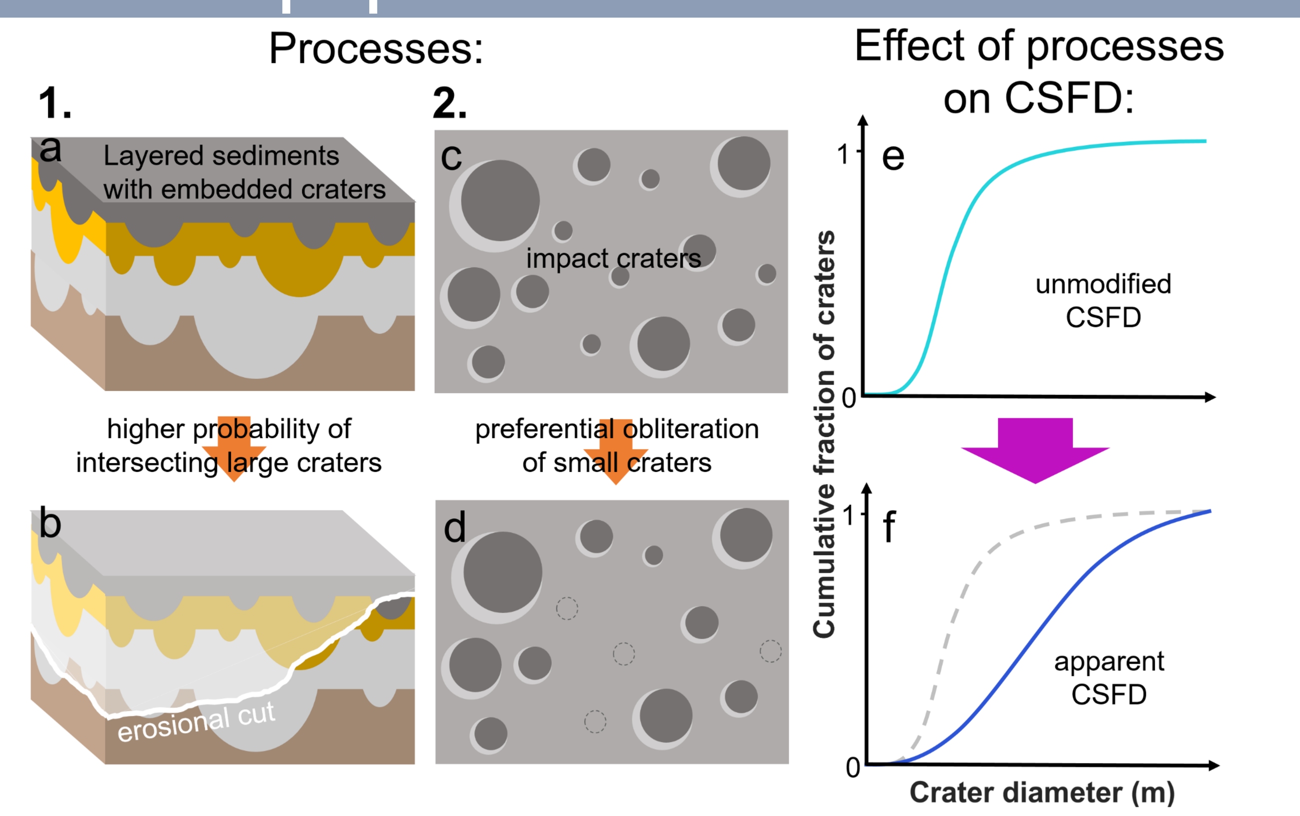

Figure 5. Schematic illustrating the effect that depositional and erosional processes have on CSFD shape. Process 1: a) initial cratered volume before modification, b) intersection of erosional cut with cratered volume, cut intersects more large craters than are represented by the underlying crater population. Process 2: c) initial cratered surface, d) cratered surface after modification by sedimentary processes with obliterated smaller craters indicated by dashed circles. Effect of processes on CSFD: e) initial CSFD for a & c (pre-modification), f) observed CSFD for b & d after modification by processes 1 & 2. The grey dashed curve is the original, unmodified CSFD from e.

Small craters are preferentially obliterated by sedimentation due to their reduced topographic expression, are less likely to be exposed by erosional cuts through a cratered volume[24]. This changes the observed crater size frequency distribution (Fig 4).

Low pressure = 0.3 bar, high pressure = 3.3 bar

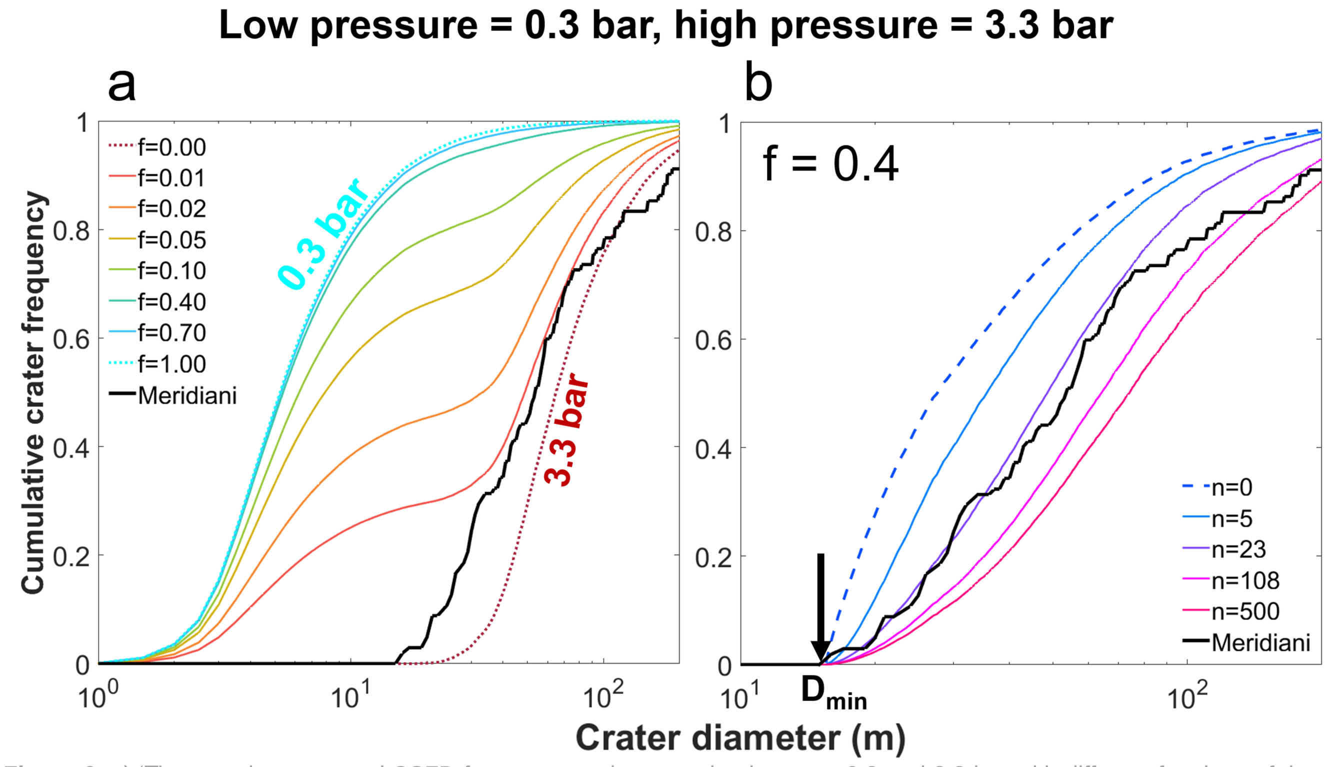

Figure 6. a) 'Time-varying pressure' CSFD for an atmosphere varying between 0.3 and 3.3 bar with different fractions of time spent at lower pressure (f). Dashed colored lines show persistent 0.3 and 3.3 bar atmospheres. Thick black line shows measured Meridiani CSFD. To illustrate the effect of simulated crater population modification on synthetic CSFDs, b) shows a 'Time-varying pressure' CSFD with f = 0.4 and different degrees of preferential obliteration of small craters (n).

Atmospheric pressure can vary during crater accumulation (Fig 5a). Our measured crater size frequency distributions can be reproduced by time-varying atmospheric pressure and preferential removal of small craters, provided that the minimum atmospheric pressure is less than our new upper limits (Fig 5b).

5. Mars paleopressure evolution

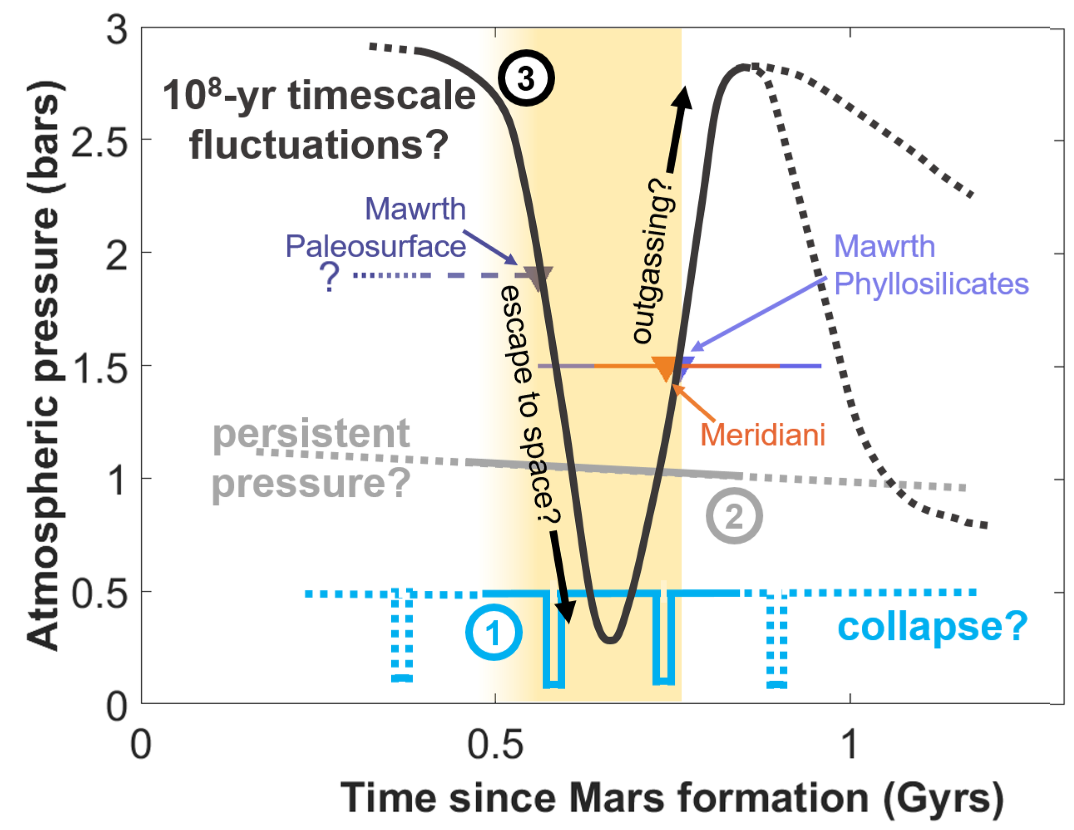

Figure 7. Schematic illustration of 3 possible end-member cases for Mars' atmospheric pressure history for ~4-3.8 Ga (yellow area). Dotted lines: pressure not directly constrained by existing data.

Our results suggest **3 end-member paleopressure histories from ~4-3.8 Ga** (Fig 7):

1. Maximum pressure <0.5 bar with episodes of condensation of CO2 into ice caps
2. Pressure persistently below our upper estimates
3. Pressure changes of several bar due to changes in atmospheric sources/sinks.

To integrate our results with existing knowledge, we built a 2-component, process-agnostic model of Mars' paleopressure evolution. We gathered sources and sinks into 1 term each, expressed as either a powerlaw: $\frac{dP_{atm}}{dt} = k_{1/3}t^{-k_{2/4}}$

or an exponential: $\frac{dP_{atm}}{dt} = k_{1/3}\exp(-k_{2/4})$

with free parameters k_1, k_2 (sinks), k_3 & k_4 (sources) found using existing paleopressure estimates. Our model is sensitive to the lowest implemented pressure constraint ([15]b or [16]b; Fig 8). However, in both cases, **most solutions give pressures <1 bar before 4 Ga.**

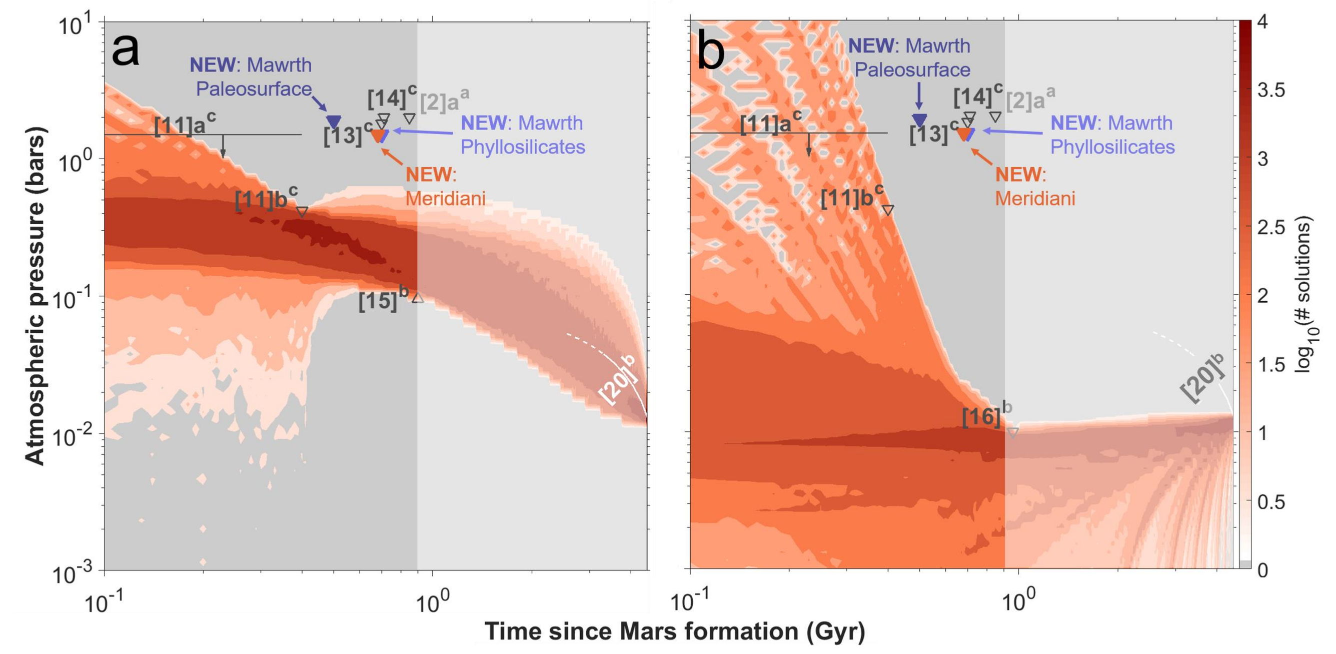

Fig 8- Paleopressure histories allowed by existing data. Solution density plots of pres-sure histories for 10,000 combinations of k_1–k_4. Grey areas do not match data. $\log_{10}$(# solutions) = all solutions pass through point. a) lowest constraint at ~3.8 Ga is [15]b b) [16]b. Constraints as for Fig 4. Washed out region - no paleopressure estimates exist 3.6 Ga - present, solutions not well constrained.

6. Future science directions

- **More paleopressure estimates are needed.** There are few paleopressure constraints 3.6 to <<1 Ga (Figs 4 & 8).
- **More precise chronologies for climate-altering events**, such as the end of the Martian dynamo and the growth of Tharsis, would constrain the feasibility of scenario 3 (Fig 7).
- **Improved dating of Martian sedimentary deposits** would reduce the uncertainty on the ages of our sites and better constrain the time intervals during which Mars had surface liquid water.

Acknowledgements: J. Sneed produced the HiRISE DTMs (pipeline: [25]). Grants: NASA (NNX16AJ38G).

References: [1] Jakosky B. M. & Phillips R. J. (2001) *Nature*, *412*, 237. [2] Kite E. S. et al. (2014) *Nat. Geosci.*, *7*, 335. [3] Tauber M. E. & Kirk D. B. (1976) *Icarus*, *208*, 351. [4] Vasavada A. R. et al. (1993) *JGR: Planets*, *98*, 3469. [5] Loizeau D. et al. (2012) *P&SS*, *72*, 31. [6] Bishop J. et al. (2018) *Nat. Astron.*, *2*, 206. [7] Hynek B. M. & Di Achille, G. (2017), *USGS Investigations Map 3356*. [8] Davis J. M. et al. (2016) *Geology*, *44*, 847. [9] Williams J.-P. et al. (2014) *Icarus*, *235*, 23-36. [10] Lammer H. et al. (2013) *SSR.*, *174*, 113. [11] Cassata W. S. et al. (2012) *Icarus*, *221*, 461. [12] Kurokawa H. et al. (2018) *Icarus*, *299*, 443-459. [13] van Berk W. et al. (2012) *JGR Planets*, *117*. [14] Hu R. et al. (2015) *Nat. Communications*, *6*. [15] Manga M. et al. (2012) *GRL*, *39*. [16] Lapôtre M. G. A. et al. 2016 *Science*, *353*, 55-58. [17] Bristow T. F. et al. (2017) *PNAS*, *114*, 2166-2170. [18] Tosca N. J. et al. (2018) *Nat. Geosci.*, *11*, 635. [19] Bierson C. J. et al. (2016) *GRL*, *43*, 4172. [20] Lillis R. J. et al. (2015) *SSR*, *195*, 357. [21] Forget F. et al. (2013) *Icarus*, *222*, 81-99. [22] Turbet et al. (2019) *Icarus*, *321*,189. [23] Jakosky B. M. (2018) *Icarus*, *315*, 146. [24] Mayer D.P. & Kite E.S. (2016) *LPSC XLVII*, abstract #1241.